www.elsevier.com/locate/memsci

Water desalination using graphene-enhanced electrospun nanofiber membrane *via* air gap membrane distillation

Yun Chul Woo, Leonard D. Tijing, Wang-Geun Shim, June-Seok Choi, Seung-Hyun Kim, Tao He, Enrico Drioli, Ho Kyong Shon

PII: S0376-7388(16)30665-2
DOI: http://dx.doi.org/10.1016/j.memsci.2016.07.049
Reference: MEMSCI14634

To appear in: *Journal of Membrane Science*

Received date: 13 June 2016
Revised date: 21 July 2016
Accepted date: 25 July 2016

Cite this article as: Yun Chul Woo, Leonard D. Tijing, Wang-Geun Shim, June-Seok Choi, Seung-Hyun Kim, Tao He, Enrico Drioli and Ho Kyong Shon Water desalination using graphene-enhanced electrospun nanofiber membrane *via* air gap membrane distillation, *Journal of Membrane Science* http://dx.doi.org/10.1016/j.memsci.2016.07.049

Water desalination using graphene-enhanced electrospun nanofiber membrane *via* air gap membrane distillation

In preparation for

Journal of Membrane Science

Yun Chul Woo[a], Leonard D. Tijing[a*], Wang-Geun Shim[b], June-Seok Choi[c], Seung-Hyun Kim[d], Tao He[e], Enrico Drioli[f], Ho Kyong Shon[a*]

[a]Centre for Technology in Water and Wastewater, School of Civil and Environmental Engineering, University of Technology Sydney (UTS). P. O. Box 123, 15 Broadway, NSW 2007, Australia

[b]Department of Polymer Science and Engineering, Sunchon National University, 255 Jungang-ro, Suncheon, Jeollanam-do, Republic of Korea

[c]Environment and Plant Research Institute, Korea Institute of Civil Engineering and Building Technology (KICT), 283, Goyangdae-Ro, Ilsanseo-Gu, Goyang-Si, Gyeonggi-Do 411-712, Republic of Korea

[d]Civil Engineering Department, Kyungnam University, Wolyoung-dong, Changwon, 631-701, Republic of Korea

[e]Laboratory for Membrane Materials and Separation Technology, Shanghai Advanced Research Institute, Chinese Academy of Sciences, Shanghai 201203, China

[f]Institute on Membrane Technology (ITM-CNR), National Research Council, c/o The University of Calabria, Cubo 17C, Via Pietro Bucci, 87036 Rende CS, Italy

Leonard.Tijing@uts.edu.au

ltjing@gmail.com

Hokyong.Shon-1@uts.edu.au

[*]Corresponding authors: L. D. Tijing, Tel: +61 2 9514 2652,

[*]Corresponding authors. H. K. Shon, Tel: +61 2 9514 2629

Abstract

This study demonstrates the preparation and desalination performance via air gap membrane distillation (AGMD) of a graphene-loaded electrospun nanofiber membrane. Different concentrations of graphene (0-10 wt%) were incorporated in/on electrospun polyvinylidene fluoride-co-hexafluoropropylene (PH) membrane to obtain a robust, and superhydrophobic nanocomposite membrane. The results showed that graphene incorporation has significantly enhanced the membrane structure and properties with an optimal concentration of 5 wt% (i.e., G5PH). Characterization of G5PH revealed membrane porosity of >88%, contact angle of >162^{o} (superhydrophobic), and high liquid entry pressure (LEP) of >186 kPa. These favourable properties led to a high and stable AGMD flux of 22.9 L/m^{2}h or LMH (compared with ~4.8 LMH for the commercial PVDF flat-sheet membrane) and excellent salt rejection (100%) for 60 h of operation using 3.5 wt% NaCl solution as feed (feed and coolant inlet temperatures of 60 and 20^{o}C, respectively). A two-dimensional dynamic model to investigate the flux profile of the graphene/PH membrane is also introduced. The present study suggests that exploiting the interesting properties of nanofibers and graphene nanofillers through a facile electrospinning technique provides high potential towards the fabrication of a robust and high-performance AGMD membrane.

graphical abstract

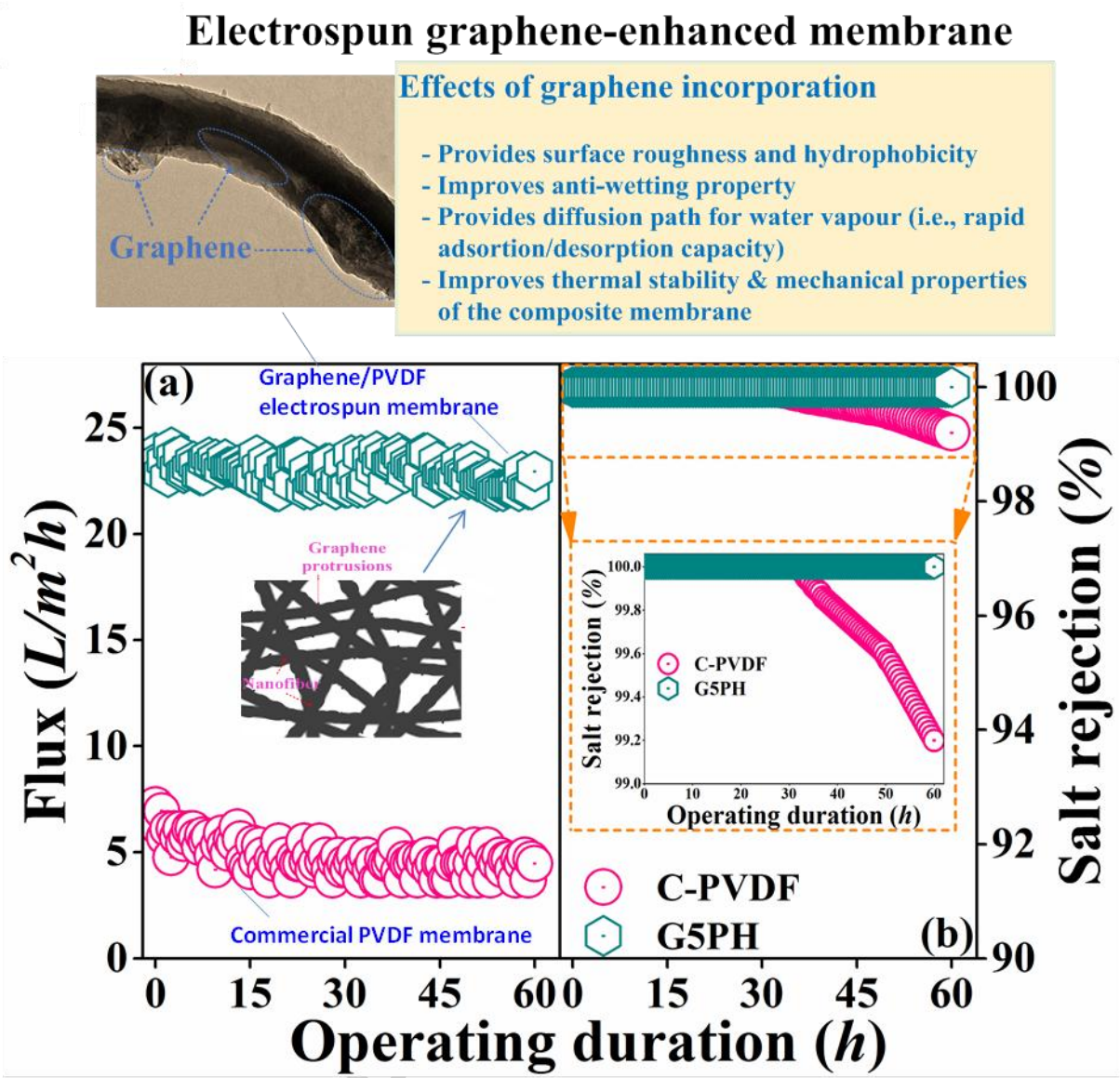

Keywords: Graphene, air gap membrane distillation, superhydrophobic, electrospun nanofiber, desalination

1. Introduction

Membrane distillation (MD) is an emerging non-isothermal membrane separation technology for treating saline and hyper saline solutions such as seawater or reverse osmosis (RO) brine [1-3]. Unlike pressure-driven processes, the driving force in MD is the partial vapour pressure difference

brought about by the temperature difference between the feed and permeate streams [4-7]. Since MD does not require high pressure, its fouling and scaling propensity is not as problematic as other processes, thus less pre-treatment is required. So MD can be made into compact systems and can even use non-corrosive and cheap plastic materials as hydraulic pressure is low. So far, it presents a very promising prospect for portable and stand-alone desalination process. However, full-scale commercialisation of MD still faces three major issues: the lack of appropriate membranes, proper and efficient module design, and intensive energy consumption (if solar, waste heat or other alternative energy source is not used). The present study addresses the first issue, i.e., the lack of appropriate membranes for MD.

MD requires a hydrophobic and porous membrane to proceed with its separation process, i.e. only allowing water vapour to pass through and not the liquid water. In most MD studies including bench-scale and pilot experiments, commercially-available flat-sheet or hollow fiber microfiltration membranes are usually employed due to their hydrophobic property, adequate pore sizes, and decent porosity. However, these microfiltration membranes are not ideally-designed for MD, thus they suffer from low permeability and wetting problem in long term performance. Hence, there is a need to design and manufacture new membranes for MD application [8-12].

Among the different membrane designs fabricated by various techniques, electrospun membranes have garnered wide interest in the recent years as potential membranes for MD due to their unique characteristics. These membranes are fabricated through an electrospinning process, wherein a high voltage is applied to a polymer solution, which is emitted into jets and form into submicron-sized fibers and collected as a non-woven flat-sheet membrane [13]. Electrospun membranes possess high hydrophobicity, high porosity, high surface area-to-volume ratio and interconnected pore structure. The overlapping structure of the nanofiber provides rough nano-scale surface which leads to increased hydrophobicity that is ideal for the MD process. In recent years, a number of research studies are reported using electrospinning for MD application [14-17]. Several polymers have been electrospun including polyvinylidene fluoride (PVDF), polyvinylidene fluoride-co-hexafluoropropylene (PVDF-*co*-HFP), and polystyrene (PS) [14, 16-19]. However, to date,

continuous research efforts are still being undertaken to manufacture a robust electrospun membrane for long term efficient MD performance. Superhydrophobic membranes are being sought out as an appropriate membrane for MD [20-23]. At having superhydrophobicity, it can lead to less wetting problem, enhanced liquid entry pressure (LEP), improved water vapour flux and high salt rejection [8, 24]. Incorporation of nanofillers such as silica and carbon nanotubes (CNTs) in/on nanofibers is reported to lead to superhydrophobic electrospun membranes.

Recently, increasing interest is given to graphene as a unique nanofiller material that has interesting properties that could provide additional functionalities to the host material. Graphene is two-dimensional (2D), single carbon atom composed of sp^2 arranged in a honeycomb structure, and is an emerging new material used in various research fields including water treatment and purification processes [25-27]. It has high thermal stability and electrical conductivity, high mechanical stiffness, low permeability to water, and is low cost [28, 29]. The very high aspect ratio and high specific surface area make graphene ideal filler that could promote better interaction with the host polymer. Water and vapour molecules cannot penetrate via pure graphene pore due to its unique nature [30]. Graphene is particularly attractive for MD application due to its hydrophobic nature, selective sorption of water vapours, and anti-fouling properties [30-32]. Recent progress on the much cheaper synthesis of graphene provides better potential for its wider use [33].

Together with the attractive properties of nanofibers, the incorporation of graphene provides additional properties to the composite membrane such as added roughness and hydrophobicity that leads to robust and highly efficient MD membrane. In the present study, we exploited the unique properties of graphene to enhance the overall properties of a polymeric nanofiber membrane towards the production of a robust superhydrophobic membrane for long-term air gap membrane distillation (AGMD) application. To the best of our knowledge, no one has reported yet on the use of graphene-incorporated electrospun nanofiber membrane for AGMD desalination. Realizing the excellent properties of graphene and electrospun nanofiber membranes, their combination as MD membrane is worth exploring. Hence, the objective of this study was to determine the optimal concentration of graphene in/on the electrospun nanocomposite membrane to lead to a robust and high AGMD

performance desalination membrane. A series of measurements, characterization and AGMD tests were performed to determine the most suitable graphene loading and membrane composition for AGMD desalination.

2. Materials and methods

2.1 Materials

PVDF-*co*-HFP (Mw = 450,000 g/mol, Kynar Powerflex® LBG) (referred herein as PH) and N, N-dimethylformamide (DMF) solvent were purchased from Arkema Inc., Australia and Sigma-Aldrich, respectively. The graphene used in the present study was xGNP-C500-grade material from XG-Science, USA, which has a particle diameter of 1 ~ 2 µm, an average thickness of 2 nm and an average surface area of 500 m^2/g. Ethanol was purchased from Ajax Finechem Pty Ltd. For AGMD performance test, sodium chloride (NaCl, Chem-supply) and deionized (DI) water were used. All chemicals were used as received. Commercial PVDF membrane (Durapore®-GVHP, pore size = 0.22 µm) received from Merck Millipore was used as a reference for AGMD flux and salt rejection performance comparison.

2.2 Dope preparation

Neat PH solution (referred herein as PH18) was prepared by dissolving 18 wt% PH in DMF/acetone solvent (4:1 ratio) via magnetic stirring overnight. For graphene/PH solutions, a given amount of graphene (1, 3, 5, 7, and 10 wt% relative to PH; referred herein as G1PH, G3PH, G5PH, G7PH and G10PH, respectively) was first dispersed in a certain amount of DMF/acetone solution by bath sonication (Thermoline Scientific) for 1 hour and then mixed with 18 wt% PH solution by magnetic stirring at 80^{o}C for another hour followed by stirring at room temperature for 24 h.

2.3 Electrospinning of superhydrophobic G/PH nanofiber membranes

The electrospinning set-up is explained in detail in our previous work [14]. All of the fabricated membranes were electrospun at an employed voltage, tip-to-collector distance, and feed flow rate of 10 kV, 100 mm, and 1.0 ml/hour, respectively (**Table S1**). All nanofibers were directly fabricated onto a rotating drum collector covered with aluminium foil. The polymer solution was supplied in a 10 ml syringe attached with a needle (21G, inner diameter = 510 µm) that was mounted

on an adaptor. The needle kept on oscillating sideways during electrospinning and was controlled by LabView software (National Instrument). The chamber humidity (40 ~ 50 %) and temperature (18 ~ 23°C) were maintained constant throughout the electrospinning process. After electrospinning, the as-spun membranes were peeled off from the aluminium foil and transferred onto a baking paper and kept in a dry oven (OTWMHD24, LABEC) at 50 °C for 1 day to remove the residual solvents.

2.4 AGMD performance test

The commercial PVDF, and neat and G/PH electrospun nanofiber membranes were operated in a home-made AGMD set-up (**Fig. 1**) with a feed channel dimension of 60 × 35 × 1 mm (L × W × H), an effective membrane area of 21 cm^2 and an air gap thickness of 3 mm. The coolant plate was made of a stainless steel to condense the water vapour. The AGMD in a co-current flow set-up was carried out with constant inlet temperatures at the feed and the coolant sides of 60 ± 1.5 °C and 20 ± 1.5 °C, respectively. The feed solution was 3.5 wt% NaCl solution (conductivity of 62.0 ± 0.5 mS/cm) and the coolant fluid was tap water. The feed and coolant circulation rates were both maintained at 12 L/h.

2.5 Characterizations of the G/PH and neat PH electrospun nanofiber membranes

The surface and cross-sectional morphologies of graphene/PVDF-co-HFP (G/PH) nanofiber samples were observed by scanning electron microscopy (SEM, Zeiss Supra 55VP, Carl Zeiss AG). Samples taken from each membrane were coated with gold. The SEM images were carried out at an accelerating voltage of 10 kV, and different image magnifications at various areas were obtained for each sample. The fibre size distribution was acquired by image analysis of several SEM images using ImageJ software (NIH).

Membrane surface roughness was analysed by atomic force microscopy (AFM) imaging. AFM was carried out under ambient conditions in tapping mode with silicon probes (TT-AFM, AFM workshop) [12].

The morphology of the pristine graphene and the G/PH nanofiber was observed by transmission electron microscopy (TEM, Tecnai T20, FEI Tecnai™). The G/PH nanofibers were placed on 200 mesh copper grid (Ted Pella Inc., CA, USA) and examined with high resolution TEM.

The contact angles of the electrospun membranes were measured using a sessile drop method by an optical subsystem (Theta Lite 100) equipped with image-processing software. Sample membranes were placed on a platform and droplets of 5-7 µL were dropped carefully on the membrane surface. A real-time camera captures the image of the droplet and the CA is estimated. At least 5 measurements were taken for each membrane sample and the average value is reported here.

The membrane porosity, defined as the volume of pores divided by the total volume of the membrane was measured via a gravimetric method [14]. Equal sizes of 3 cm x 3 cm membrane samples were immersed in ethanol. The weight of the samples was measured before and after saturation of ethanol, and the membrane porosity was determined by the following equation:

$$\rho = \frac{(W_1 - W_2)/D_e}{[(W_1 - W_2)/D_e] + W_2/D_p} \quad (1)$$

where ρ is the porosity, W_1 is the weight (g) of the saturated membrane, W_2 is the weight (g) of the dry membrane, D_e is the density (g/m^3) of the ethanol (Ajax Finechem Pty Ltd) and D_p is the overall density (g/m^3) of PH material.

Liquid entry pressure (LEP), which is a measure of the ability of a hydrophobic membrane against pore wetting, was investigated using a homemade LEP set-up as shown in our previous work [27]. The reservoir was first filled with 25 ml distilled water and then a dry membrane sample (effective surface area = 7 cm^2) was tightly secured in the cell. Nitrogen gas was then supplied to the bottom of a silicone cork in the water-filled chamber, raising the pressure step wise, thereby pushing the water up to the membrane sample. The first sign of bubble on the top of the membrane was regarded as the LEP. To reduce the error, triplicate measurements were taken and averaged.

The pore size and pore size distribution (PSD) of the commercial and nanofiber membranes were measured by capillary flow porometry (Porolux 1000). All samples were first applied with N_2 gas to determine the gas permeability and then the dry samples were wetted by Porefil (a wetting liquid with a low surface tension of 16 dynes/cm) and tested under the same condition. The mean pore size of the samples was calculated from wet, dry and half dry conditions [27].

The mechanical properties of the different membrane samples were measured using a Universal Testing Machine (UTM LS, Lloyd), equipped with a 1 kN load cell. The test was conducted using a constant elongation velocity of 5 mm/min under room temperature.

The material analysis was done by attenuated total reflectance Fourier transform infrared spectroscopy (ATR-FTIR) via Paragon 1000 Spectrometer (PerkinElmer, USA) in the range of 500-4000 cm^{-1} with a signal resolution of 1 cm^{-1} and a minimum of 16 scans. X-Ray diffraction (XRD) (Siemens D5000) was carried out over Bragg angles ranging from 6° to 60° (Cu Kα, λ=1.54059Å). Raman spectra of the membranes were obtained via a Renishaw in Via Raman spectrometer system (Renishaw, Gloucestershire, UK) using a He-Ne laser source at 633 nm with a spectral resolution of 1 cm^{-1}. Thermogravimetric analysis (TGA) was carried out using a Q600 (TA Instuments). The fabricated membranes were heated to 1000°C at a rate of 10°C/min in N_2.

In order to investigate the textural properties of the PVDF membrane and graphene composite PVDF membrane, the well-known nitrogen adsorption/desorption experiments were performed at 77 K using the nanoPOROSITY adsorption analyzer (Mirae SI, Korea). Before the test, the samples were degassed in vacuum for 24 h to eliminate the surface contaminants including the moisture. The textural properties including specific surface area, pore volume, pore size distributions were determined using the Brunauer–Emmett–Teller (BET) and the Barrett–Joyner–Halenda (BJH) methods. In addition, the nitrogen adsorption energy distributions were calculated using the generalized nonlinear regularization method [34-36].

3. Results and discussion

3.1 Membrane characteristics and morphology

The characteristics and morphologies of the neat and G/PH electrospun nanofiber membranes are shown in **Table 1 and Fig. S1**. All of the fabricated membranes showed highly-porous, non-woven and overlapping nanofiber structures and had a similar thickness of about 100 μm. The mean and maximum pore sizes of the electrospun membranes did not change much even with the incorporation of different graphene concentrations. However, it could be seen that the fiber diameter decreased with the incorporation of graphene compared with the neat PH until 3wt% graphene

concentration, and then increased slightly at higher concentrations. This decreasing fiber diameter trend could be attributed to the increased conductivity of the graphene/PH solutions, which increased the likelihood of more electrostatic repulsion leading to increased stretching, hence smaller fibers. At higher graphene concentration (>3 wt%), this could have led to increased viscosity and more agglomeration among graphene particles [27], which led to bigger fiber diameters, as also observed by other studies [37, 38].

The decreasing porosity from 94.7% for neat PH to 82.3% for G10PH was mainly because of the existence of aggregated graphene and some bead formation on the membrane surface at increasing graphene concentrations (**Figs. S1** and **S2**). However, it should be noted that regardless of the decreasing porosity of the graphene/PH membranes, they still have much higher porosity compared with the commercial PVDF membrane (~70%). This high porosity of nanofiber membrane is an attractive asset for MD application as higher porosity indicates more surfaces for vapour to pass through, hence enhanced flux rate [15]. Though the mean pore and maximum pore sizes were similar for all electrospun membranes, the graphene-loaded membranes showed increasing LEP values from 163 kPa for G1PH to 190 kPa for G10PH, compared with 139 kPa for neat PH. This clearly shows that graphene has enhanced the anti-wetting property of the membrane, which could be attributed to the added hydrophobicity of the incorporated graphene, as confirmed by contact angle (CA) measurements (**Table 1** and **Fig. 2**), showing increased CAs (149 to 162^{o}) with increasing graphene contents up to 5 wt%. In **Fig. 3**, AFM results of the nanofiber membranes revealed that G5PH membrane had much rougher mean surface roughness (R_a= 0.719 ± 0.03 µm) compared with that of neat PH18 membrane (R_a= 0.623 ± 0.013 µm), which is attributed to the added roughness from the graphene nanoparticles in/on the nanofiber. Slight decrease in CA was observed at >5wt% graphene content which could be due to more agglomeration of graphene that led to less and non-uniform dispersion of graphene on the membrane surface (**Fig. S2**). Though some researchers noted that the ideal pore size for MD membrane should be <0.6 µm to avoid wetting problems, however, this is not the case with our present study, as also observed by other researchers utilising nanofiber membranes mainly due to increased hydrophobicity of electrospun membrane. For example, Liao et al. observed

no wetting problems for 50 h of their nanofiber membranes despite having bigger pores (i.e., >0.6 μm) [15]. It should be noted that the wetting phenomenon is not only affected by the pore size, but by different membrane properties such as hydrophobicity, pore size distribution, and operating parameters. Based from **Table 1**, the optimal graphene concentration was found to be 5 wt%, obtaining the highest CA and favourable porosity and LEP values.

Further checking of G5PH (see **Fig. 4(a)** and **Fig. 4(b)**) showed interconnected and overlapping fibers, with graphene sheets protruding at the surface. Characterization by TEM (**Fig. 4(c**)) also revealed the successful incorporation of graphene with many protruding on the surface leading to nano surface roughness and higher hydrophobicity.

EDX measurement was carried out to further confirm the successful incorporation of graphene in/on the nanofiber (**Fig. 5). Figure 5(a)** indicates increasing atomic carbon concentration with the increase in the amount of graphene incorporated in/on the membrane, suggesting the presence of more graphene at increasing concentration. The atomic carbon to fluorine (C/F) ratio (**Fig. 5(b)**) also showed increasing values with the increase in graphene contents, further confirming the proper dispersion and incorporation of graphene.

3.2 Structural and chemical characterization

Figure 6 shows the results of XRD, FT-IR and Raman spectroscopy measurements of the fabricated membranes. XRD crystallographic analyses (**Fig. 6(a)**) reveal that PH is crystalline showing peaks at 18.5º and 20.5º, which correspond to α (0 2 0) and β ((2 0 0)/(1 1 0)) crystal phases, respectively [39]. This indicates the existence of both α and β phases. Meanwhile, G5PH membrane showed an additional peak at 26.4º [40], which is the characteristic peak of graphene (see **Fig. 6(b)**), indicating the presence of graphene in the composite membrane. G5PH showed slight shifting of the peaks to the left which suggests the interaction between the polymer matrix and graphene nanofiller.

Fig. 6(c) shows the FT-IR spectra of the different fabricated membranes. All neat and G/PH nanofibers showed the same absorption bands attributed to the basic structural characteristics of PVDF-HFP at 839 cm^{-1}, 879 cm^{-1}, 1072 cm^{-1}, 1178 cm^{-1}, 1269 cm^{-1}, and 1400 cm^{-1}, which correspond to CH_2 rocking and CF_2 asymmetric stretch (the β phase), CH_2 in plane bending or rocking (the α

phase), C-C asymmetric stretch, C-C asymmetric stretch and CF_2 symmetric stretching, CF out of plane deformation (the β phase), and CF stretching vibrations or CH_2 wagging (the α phase), respectively [41]. Similar spectra were observed for the G/PH electrospun membranes but at lower intensities, which signify the presence of interfacial interaction (physical adsorption or weak chemical bonding) between PH and graphene particles.

The Raman spectra of G5PH electrospun membrane (**Fig. 6(d))** showed two prominent peaks at 1340 and 1580 cm^{-1}, which are indicative of the D (defect-induced region) and G (ordered lattice or in-plane vibrations of carbon atoms) bands of graphene, respectively [42]. This suggests the presence of graphene in the membrane. The D and G band intensity ratio (I_D/I_G) or the R-value of the graphene powder and that of G5PH was very similar (0.86 and 0.95, respectively) indicating that graphene in the composite membrane has maintained its chemical structure and crystallinity [43].

3.3 Thermal and mechanical properties of the G/PH membrane

The thermal and mechanical properties of the samples were measured by TGA and tensile tester, respectively, and the results are shown in **Fig. 7** and **Table 1**. It is general knowledge that when nanofillers are properly dispersed in a host polymer, they can spread the load transfer of the composite material, thereby improving its thermal and mechanical properties. In the present study, the incorporation of 5 wt% graphene in/on PH nanofiber has resulted to improved thermal and mechanical properties. Based from the TGA curves in **Fig. 7(a)**, the neat PH membrane showed two prominent weight losses at ~ 146ºC and at ~ 400ºC, which are consistent with the degradation pattern of PVDF-*co*-HFP [44]. For G5PH membrane, a shift of thermal decomposition towards higher temperature (about 14^{o}C higher) was observed, which confirms enhancement in thermal stability. The weight loss of the neat PH and the G5PH electrospun nanofiber membranes at 480ºC was 38.6% and 46.5%, at 600ºC was 30.8% and 36.1%, and at 700ºC was 28.3% and 33.0%, respectively. Higher residual mass was observed for G5PH compared with neat PH at 1000^{o}C indicating the good dispersion of graphene in the composite membrane that resulted to improved thermal properties. As observed in SEM and TEM, graphene was either fully enveloped in the polymer matrix or protruding while the tail end is embedded onto the nanofiber [45].

The MD process is commonly employed under atmospheric pressure so that the membrane for MD has lower requirements for tensile properties, however, adequate tensile properties are still needed to guarantee successful packing in modules and to provide stable operation [46]. Thus, the mechanical properties of the membranes were investigated.

Fig. 7(b) shows the stress-strain curves of the commercial and electrospun membranes. Neat PH nanofiber exhibited a tensile strength and elongation of 8.1 MPa and 102.4%, respectively. Meanwhile, G5PH exhibited tensile strength and elongation of 12.2 MPa and 143.9%, respectively, or an increase of 51% in tensile strength when graphene was incorporated. Even elongation has increased for G5PH compared with neat PH. This clearly indicates the good interaction of graphene and PH polymer matrix that resulted to good load transfer from PH to graphene. Membranes with higher graphene loading (> 7 wt%) have decreased mechanical properties compared with the G5PH membrane, which shows that the graphene loading of 5 wt% is optimum (**Table 1**). Additionally, the increased mechanical property of G5PH could be due to good interfacial interaction between graphene and polymer matrix, weak van der Waals bonding between PH and graphene, and some micromechanical locking of fibers and graphene. Interestingly, the nanofiber membranes posted much better tensile strength and elongation compared with the commercial PVDF flat-sheet membrane (7.2 MPa and 36.3%, respectively). The stress-strain curves of the nanofiber membrane and commercial membrane presented different trends. The commercial membrane had a steep increase in tensile strength in the first 10% elongation, and then gradually increased thereafter until failure. However, the nanofiber membrane showed a linear mode of stress-strain curve, which could be attributed to the nonwoven structure of the nanofibers as compared to a more dense structure of the commercial membrane.

3.4 BET of the G/PH membrane

Nitrogen adsorption/desorption analysis was used to further characterize the neat PH and graphene composite membrane, G5PH. As shown in **Fig. 8(a)**, both neat PH and G5PH represent typical type II or III isotherms with type H3 (or H4) hysteresis loop and sharp increase in adsorption at a high relative pressure of 0.9-0.99, representing the existence of the numerous meso and

macropores in the sample [47, 48]. This nitrogen adsorption analysis reveals that the graphene composite membrane, G5PH, has a relatively larger surface area and pore volume compared with those of neat PH, revealing appreciable development of the porosity after introducing the graphene into membrane. Namely, G5PH represent a specific surface area of 163 m^2/g with a total pore volume of 0.379 cm^3/g, which is about 2 to 3 times greater than those of PH (78 m^2/g and 0.131 cm^3/g). However the specific surface area of G5PH is approximately 16 times smaller than the theoretical value (2620 m^2/g) of single layer graphene sheets.

Figure 8(b) compares the Barrett–Joyner-Halenda (BJH) pore size distribution curves derived from the desorption branches of the isotherms. These curves also indicate that G5 has more plentiful amounts of meso pores than those of PH, which are closely related to the graphene sheets (See **Fig. 4(b)**, wavy wrinkles). The obtained PSD curves are uniformly distributed at 2.5 nm for G5PH and 2.9 nm for PH, respectively.

In order to comparatively examine the surface energetic heterogeneity for model membranes, nitrogen adsorption energy distribution (AED) functions were calculated using a regularization method. In this work, the Flower-Guggenheim isotherm model was used as a kernel function because this equation can generally explain the localized adsorption with lateral interactions [34, 35, 49, 50]. As compared in **Fig. 8(c)**, the shapes of AED function curve for neat PH and G5PH differ slightly, providing further evidence of the existence of different types of surface energy. The G5PH represent two pronounced peaks at 4.3 and 13.4 kJ/mol (see inset) but the neat PH shows only a single peak at 4.2 kJ/mol. No appreciable high energy peak is obtained in the neat PH. These results clearly indicate that the G5PH have mainly two different types of surface energetic heterogeneity for nitrogen. In particular, the high-energy peak observed in G5PH can be explained with the existence of the graphene nanosheets in the composites, which can provide more suitable pores and available adsorption sites for target ion. Thus it is reasonable to suggest that the graphene composite, G5PH, seems to be more heterogeneous than that of neat PH.

3.5 AGMD performance of the G/PH membranes

Figure 9 presents the AGMD performances of the different fabricated neat and composite membranes. Initial AGMD tests for 20 h reveal that neat PH (PH18) and G1PH membranes had wetting problems in less than 3 h of operation. However, at higher graphene loadings (>5 wt%), nearly stable fluxes were observed. The highest flux was obtained using G5PH, which was stable for 20 h at 22.91 L/m^{2}h or LMH, followed by G7PH (~18 LMH) and G10PH (~13.5 LMH), and their salt rejection was >99.99%. The difference in their performance could be explained by investigating their morphologies and properties. Although G10PH had the highest LEP among all nanofiber membranes, many agglomerations on the membrane surface could have constricted the membrane pores (which explains the high LEP) thereby decreasing the surface area for vapour transport. Similarly, G7PH showed some agglomerations at the surface but at a lesser extent compared with G10PH. The G5PH seemed to have the good dispersion of graphene in/on the surface with adequate roughness and surface pore size and porosity, thereby attaining the highest flux and high rejection.

Based from the result of the short term AGMD performance, G5PH membrane was compared to a commercial PVDF membrane for 60 h of operation and the results are shown in **Fig. 10.** The water vapour flux of the commercial membrane showed an initial value of 6 LMH and declined slightly until 15 h, then maintained constant until 60 h at 4.75 LMH. On the other hand, G5PH membrane remained stable for 60 h at 22.91 LMH. This flux is five times higher than that of the commercial membrane while maintaining a 100% salt rejection (compared with 99.2% for the commercial membrane). This better performance is attributed to the greater void volume fraction of G5PH, bigger pore sizes yet with high LEP values primarily due to superhydrophobicity, and the presence of graphene.

As shown in **Fig. 4** and depicted in **Fig. 11,** graphene addition produces multi-level roughness on the membrane surface, which helps in increasing the hydrophobicity and consequently the LEP. The large aspect ratio of graphene leads to protrusion on the surface of the nanofibers after electrospinning. When the membrane is exposed to the feed solution (see **Fig. 11**), the nano and micro-level thickness and superhydrophobicity prevent the penetration of water molecules into the membrane pores, and with the high volume fraction of electrospun membrane, allows more water

vapour to pass through. Additionally, the protruded graphene provides diffusion path for water vapour due to its rapid adsorption/desorption capacity. This adds to the overall water vapour transport across the membrane.

To further explain the role of graphene in the enhancement of AGMD performance, an experimental and theoretical evaluation is presented in the next section.

3.6 Comparison of mass transfer resistance with/without graphene

Fig. 12 compares the experimental and simulation results for G5PH and commercial PVDF. A considerable improvement in flux enhancement was obtained from G5PH. As shown in this figure, the average flux (22.91 L/m^{2}h) through G5PH is approximately 4.8 times greater than that (4.75 L/m^{2}h) of the commercial PVDF sample, which is closely related to the existence of graphene. This enhanced flux performance of G5PH can be explained by its high hydrophobicity, high thermal conductivity, large available surface area and pore volume.

The water vapor flux through the hydrophobic membrane pores can be written as follows [51].

$$J = C(P_H - P_C) \quad (1)$$

where J is the flux, C is the membrane mass transfer (or membrane distillation) coefficient, which can be described by different models, and P_H and P_C are the water vapour pressures on both channels of the membrane surface, which can be calculated using the Antoine equation, respectively (**See Supporting Table S2**). On the other hand, the total mass transfer resistance in AGMD system, R_{AGMD}, can be expressed in terms of the combined membrane resistance and air gap resistance [52]. Then the net water flux, J_{AGMD}, can be described as follows,

$$J_{AGMD} = C_{AGMD}(P_H - P_C) = \frac{1}{R_{AGMD}} = \left(\frac{1}{(R_K + R_M + R_{M-air})}\right)(P_H - P_C) \quad (2)$$

where C_{AGMD}, R_K, R_M, and $R_{M\text{-}air}$ are the mass transfer coefficient, the Knudsen diffusion resistance, the molecular diffusion resistance and the molecular diffusion resistance in the air gap, respectively (**See Supporting Table S3**). The more detailed equations for the AGMD process are given in **Supporting Sec. S1**.

Based on the heat and mass transfer equations suggested in this area, the experimental flux behavior of commercial PVDF can be well explained as shown in **Fig. 12(a)**. However, the general AGMD model could not fit the flux pattern of G5PH properly (See **Fig. 12(b)** dashed line). A considerable difference was noted between the experimental data and the predicted one, indicating the limitation of the general AGMD model. Thus in order to explain the flux behavior, in this work, we introduce the net water flux, $J_{AGMD\text{-}G}$, which consider the existence of graphene sheets as follows,

$$J_{AGMD-G} = C_{AGMD-G}\left(P_H - P_C\right) = \frac{1}{R_{AGMD-G}} = \left(\frac{1}{\left(R_K + R_M + R_{M-air}\right)} + \frac{1}{R_G}\right)\left(P_H - P_C\right) \quad (3)$$

where $C_{AGMD\text{-}G}$ and R_G are the mass transfer coefficient and the molecular diffusion resistance related with the graphene sheets, respectively. Here we used the coefficient R_G as adjustable parameter to fit the experimental flux data. As shown in **Fig. 12(b)**, a reasonable fitting to the data could be obtained using this approach, which indicates that the suggested model can describe the mass transfer process well. Moreover, **Fig. 12(c)** compares the determined membrane distillation coefficient (MDC) values for different mass transfer models, which shows the following order: Knudsen diffusion > molecular diffusion > graphene sheet > molecular air gap diffusion-air. It is clear from this result that the influence of graphene sheet on the AGMD process is larger than that of molecular air gap diffusion.

Herein, we have shown the positive effect of the incorporation of 5 wt% graphene into PH electrospun membrane for AGMD application. For further improvement, optimization of the membrane thickness and pore size distribution could be carried out in future research.

4. Conclusion

In summary, graphene/PVDF-HFP (G/PH) membranes were successfully fabricated by a one-step electrospinning technique and evaluated by air gap membrane distillation (AGMD) using 3.5 wt% NaCl solution as feed. Graphene nanoparticles have been dispersed well in/on the nanofiber, which was confirmed by FT-IR, XRD, EDX and Raman spectroscopy. Further, there was an increase in hydrophobicity of G/PH electrospun nanofiber membrane compared with the as-spun neat PH membrane. Several protruding graphene nanoparticles were observed on the nanofiber by SEM and TEM, which leads to increased contact angle. The nanofiber membrane with 5 wt% graphene loading

(G5PH) showed an adequate porosity (88.7%), pore size (0.86 μm), contact angle (162.7°) and LEP (186.9 kPa) for AGMD application. For 60 h AGMD test, G5PH nanofiber membrane showed more stable flux (22.9 LMH) and better salt rejection performances (99.99%) compared with commercial PVDF membrane (flux of 4.75 LMH and salt rejection of 99.20%). Additionally, the effect of graphene on the flux performance was corroborated by theoretical models as suggested in the present study. The present results suggest that the graphene-incorporated nanofiber membrane has good potential as a robust MD membrane for water desalination by AGMD process.

Acknowledgments

This research was supported by a grant (16IFIP-B065893-04) from the Industrial Facilities & Infrastructure Research Program funded by Ministry of Land, Infrastructure and Transport of Korean government. The authors also acknowledge the grant from the ARC Future Fellowship (FT140101208).

References

[1] M. Elimelech, W.A. Phillip, The Future of Seawater desalination- energy, technology, and the environment, Science, 333 (2011) 712-717.

[2] M.A. Shannon, P.W. Bohn, M. Elimelech, J.G. Georgiadis, B.J. Marinas, A.M. Mayes, Science and technology for water purification in the coming decades, Nature, 452 (2008) 301-310.

[3] J.H. Kim, S.H. Park, M.J. Lee, S.M. Lee, W.H. Lee, K.H. Lee, N.R. Kang, H.J. Jo, J.F. Kim, E. Drioli, Y.M. Lee, Thermally rearranged polymer membranes for desalination, Energy Environ. Sci., 9 (2016) 878-884.

[4] M. Xie, L.D. Nghiem, W.E. Price, M. Elimelech, A forward osmosis-membrane distillation hybrid process for direct sewer mining: system performance and limitations, Environ Sci Technol, 47 (2013) 13486-13493.

[5] K.R. Zodrow, E. Bar-Zeev, M.J. Giannetto, M. Elimelech, Biofouling and microbial communities in membrane distillation and reverse osmosis, Environ Sci Technol, 48 (2014) 13155-13164.

[6] S. Lin, N.Y. Yip, T.Y. Cath, C.O. Osuji, M. Elimelech, Hybrid pressure retarded osmosis-membrane distillation system for power generation from low-grade heat: thermodynamic analysis and energy efficiency, Environ Sci Technol, 48 (2014) 5306-5313.

[7] M. Yao, Y.C. Woo, L.D. Tijing, W.-G. Shim, J.-S. Choi, S.-H. Kim, H.K. Shon, Effect of heat-press conditions on electrospun membranes for desalination by direct contact membrane distillation, Desalination, 378 (2016) 80-91.

[8] L.D. Tijing, J.-S. Choi, S. Lee, S.-H. Kim, H.K. Shon, Recent progress of membrane distillation using electrospun nanofibrous membrane, Journal of Membrane Science, 453 (2014) 435-462.

[9] F.E. Ahmed, B.S. Lalia, R. Hashaikeh, A review on electrospinning for membrane fabrication: Challenges and applications, Desalination, 356 (2015) 15-30.

[10] P. Wang, T.-S. Chung, Recent advances in membrane distillation processes: Membrane development, configuration design and application exploring, Journal of Membrane Science, 474 (2015) 39-56.

[11] P. Wang, T.S. Chung, A new-generation asymmetric multi-bore hollow fiber membrane for sustainable water production via vacuum membrane distillation, Environ Sci Technol, 47 (2013) 6272-6278.

[12] L.D. Tijing, Y.C. Woo, W.-G. Shim, T. He, J.-S. Choi, S.-H. Kim, H.K. Shon, Superhydrophobic nanofiber membrane containing carbon nanotubes for high-performance direct contact membrane distillation, Journal of Membrane Science, 502 (2016) 158-170.

[13] Y.C. Woo, L.D. Tijing, M.J. Park, M. Yao, J.-S. Choi, S. Lee, S.-H. Kim, K.-J. An, H.K. Shon, Electrospun dual-layer nonwoven membrane for desalination by air gap membrane distillation, Desalination, 10.1016/j.desal.2015.09.009 (2015).

[14] L.D. Tijing, Y.C. Woo, M.A.H. Johir, J.-S. Choi, H.K. Shon, A novel dual-layer bicomponent electrospun nanofibrous membrane for desalination by direct contact membrane distillation, Chemical Engineering Journal, 256 (2014) 155-159.

[15] Y. Liao, R. Wang, A.G. Fane, Fabrication of bioinspired composite nanofiber membranes with robust superhydrophobicity for direct contact membrane distillation, Environ Sci Technol, 48 (2014) 6335-6341.

[16] Y. Liao, C.H. Loh, R. Wang, T. Fane, Electrospun superhydrophobic membranes with unique structures for membrane distillation, ACS applied materials & interfaces, 10.1021/am503968n (2014).

[17] X. Li, C. Wang, Y. Yang, X. Wang, M. Zhu, B.S. Hsiao, Dual-biomimetic superhydrophobic electrospun polystyrene nanofibrous membranes for membrane distillation, ACS Appl Mater Interfaces, 6 (2014) 2423-2430.

[18] Z. Cui, E. Drioli, Y.M. Lee, Recent progress in fluoropolymers for membranes, Progress in Polymer Science, 39 (2014) 164-198.

[19] Z. Cui, N.T. Hassankiadeh, Y. Zhuang, E. Drioli, Y.M. Lee, Crystalline polymorphism in poly(vinylidenefluoride) membranes, Progress in Polymer Science, 51 (2015) 94-126.

[20] X. Wei, B. Zhao, X.-M. Li, Z. Wang, B.-Q. He, T. He, B. Jiang, CF4 plasma surface modification of asymmetric hydrophilic polyethersulfone membranes for direct contact membrane distillation, Journal of Membrane Science, 407-408 (2012) 164-175.

[21] B.N. Sahoo, B. Kandasubramanian, Recent progress in fabrication and characterisation of hierarchical biomimetic superhydrophobic structures, RSC Advances, 4 (2014) 22053.

[22] C. Yang, X.-M. Li, J. Gilron, D.-f. Kong, Y. Yin, Y. Oren, C. Linder, T. He, CF4 plasma-modified superhydrophobic PVDF membranes for direct contact membrane distillation, Journal of Membrane Science, 456 (2014) 155-161.

[23] M. Tian, Y. Yin, C. Yang, B. Zhao, J. Song, J. Liu, X.-M. Li, T. He, CF4 plasma modified highly interconnective porous polysulfone membranes for direct contact membrane distillation (DCMD), Desalination, 369 (2015) 105-114.

[24] E.-J. Lee, A.K. An, T. He, Y.C. Woo, H.K. Shon, Electrospun nanofiber membranes incorporating fluorosilane-coated TiO2 nanocomposite for direct contact membrane distillation, Journal of Membrane Science, 10.1016/j.memsci.2016.07.019 (2016).

[25] F. Perreault, A. Fonseca de Faria, M. Elimelech, Environmental applications of graphene-based nanomaterials, Chem Soc Rev, 10.1039/c5cs00021a (2015).

[26] E.N. Wang, R. Karnik, Water desalination: Graphene cleans up water, Nat Nanotechnol, 7 (2012) 552-554.

[27] Y.C. Woo, Y. Kim, W.-G. Shim, L.D. Tijing, M. Yao, L.D. Nghiem, J.-S. Choi, S.-H. Kim, H.K. Shon, Graphene/PVDF flat-sheet membrane for the treatment of RO brine from coal seam gas produced water by air gap membrane distillation, Journal of Membrane Science, 513 (2016) 74-84.

[28] D. Cohen-Tanugi, J.C. Grossman, Water desalination across nanoporous graphene, Nano Lett, 12 (2012) 3602-3608.

[29] D. Li, R.B. Kaner, Graphene-Based Materials, Science, 320 (2008) 1170.

[30] K. Celebi, J. Buchheim, R.M. Wyss, A. Droudian, P. Gasser, I. Shorubalko, J.-I. Kye, C. Lee, H.G. Park, Ultimate Permeation Across atomically thin porous graphene, Science, 344 (2014) 289.

[31] B. Mi, Graphene Oxide Membranes for ionic and molecular sieving, Science, 343 (2014) 740.

[32] S.P. Surwade, S.N. Smirnov, I.V. Vlassiouk, R.R. Unocic, G.M. Veith, S. Dai, S.M. Mahurin, Water desalination using nanoporous single-layer graphene, Nat Nanotechnol, 10 (2015) 459-464.

[33] E.O. Polat, O. Balci, N. Kakenov, H.B. Uzlu, C. Kocabas, R. Dahiya, Synthesis of Large Area Graphene for High Performance in Flexible Optoelectronic Devices, Scientific Reports, 5 (2015) 16744.

[34] W.G. Shim, J.W. Lee, S.C. Kim, Analysis of catalytic oxidation of aromatic hydrocarbons over supported palladium catalyst with different pretreatments based on heterogeneous adsorption properties, Applied Catalysis B: Environmental, 84 (2008) 133-141.

[35] S.W. Nahm, W.G. Shim, Y.-K. Park, S.C. Kim, Thermal and chemical regeneration of spent activated carbon and its adsorption property for toluene, Chemical Engineering Journal, 210 (2012) 500-509.

[36] T. Roths, M.Martha, J. Weesec, J. Honerkamp, A generalized regularization method for nonlinear ill-posed, Computer Physics Communications, 139 (2001) 279–296.

[37] R. Moradi, J. Karimi-Sabet, M. Shariaty-Niassar, M. Koochaki, Preparation and Characterization of Polyvinylidene Fluoride/Graphene Superhydrophobic Fibrous Films, Polymers, 7 (2015) 1444-1463.

[38] C. Drew, X. Wang, L.A. Samuelson, J. Kumar, The Effect of Viscosity and Filler on Electrospun Fiber Morphology, Journal of Macromolecular Science, Part A, 40 (2003) 1415-1422.

[39] A. Baji, Y.-W. Mai, M. Abtahi, S.-C. Wong, Y. Liu, Q. Li, Microstructure development in electrospun carbon nanotube reinforced polyvinylidene fluoride fibers and its influence on tensile strength and dielectric permittivity, Composites Science and Technology, 88 (2013) 1-8.

[40] Q. An, F. Lv, Q. Liu, C. Han, K. Zhao, J. Sheng, Q. Wei, M. Yan, L. Mai, Amorphous vanadium oxide matrixes supporting hierarchical porous Fe3O4/graphene nanowires as a high-rate lithium storage anode, Nano Lett, 14 (2014) 6250-6256.

[41] Y.C. Woo, J.J. Lee, L.D. Tijing, H.K. Shon, M. Yao, H.-S. Kim, Characteristics of membrane fouling by consecutive chemical cleaning in pressurized ultrafiltration as pre-treatment of seawater desalination, Desalination, 369 (2015) 51-61.

[42] S.P. Surwade, S.N. Smirnov, I.V. Vlassiouk, R.R. Unocic, G.M. Veith, S. Dai, S.M. Mahurin, Water desalination using nanoporous single-layer graphene, Nat Nanotechnol, 10.1038/nnano.2015.37 (2015).

[43] F. Tuinstra, J.L. Koenig, Raman Spectrum of Graphite, The Journal of Chemical Physics, 53 (1970) 1126.

[44] J. Cao, B. Zhu, G. Ji, Y. Xu, Preparation and characterization of PVDF–HFP microporous flat membranes by supercritical CO2 induced phase separation, Journal of Membrane Science, 266 (2005) 102-109.

[45] K. Gethard, O. Sae-Khow, S. Mitra, Water desalination using carbon-nanotube-enhanced membrane distillation, ACS Appl Mater Interfaces, 3 (2011) 110-114.

[46] M. Essalhi, M. Khayet, Surface segregation of fluorinated modifying macromolecule for hydrophobic/hydrophilic membrane preparation and application in air gap and direct contact membrane distillation, Journal of Membrane Science, 417-418 (2012) 163-173.

[47] F. Rouquerol, J. Rouqueorol, K. Sing, Adsorption by Powders and Porous Solids: Principles, methodology, and applications, San Diego: Academic Press, 1999.

[48] S. Lowell, J.E. Shields, M.A. Thomas, M. Thommes, Characterization of Porous Solids and Powders: Surface Area, Pore Size and Density, Springer Netherlands, 2004.

[49] M. Jaroniec, R. Madey, Physical Adsorption on Heterogeneous Solids, Elsevier, Amsterdam, 1988.

[50] W. Rudzinski, D. Everett, Adsorption of Gases on Heterogeneous Solid Surfaces, Academic Press, London, 1991.

[51] H. Geng, H. Wu, P. Li, Q. He, Study on a new air-gap membrane distillation module for desalination, Desalination, 334 (2014) 29-38.

[52] E. Drioli, A. Ali, F. Macedonio, Membrane distillation: Recent developments and perspectives, Desalination, 356 (2015) 56-84.

Figure 1 Schematic diagram of AGMD process: (a) cooling circulation bath, (b) coolant tank, (c) water permeate tank, (d) balance, (e) AGMD module, (f) feed tank, and (g) heating circulation bath

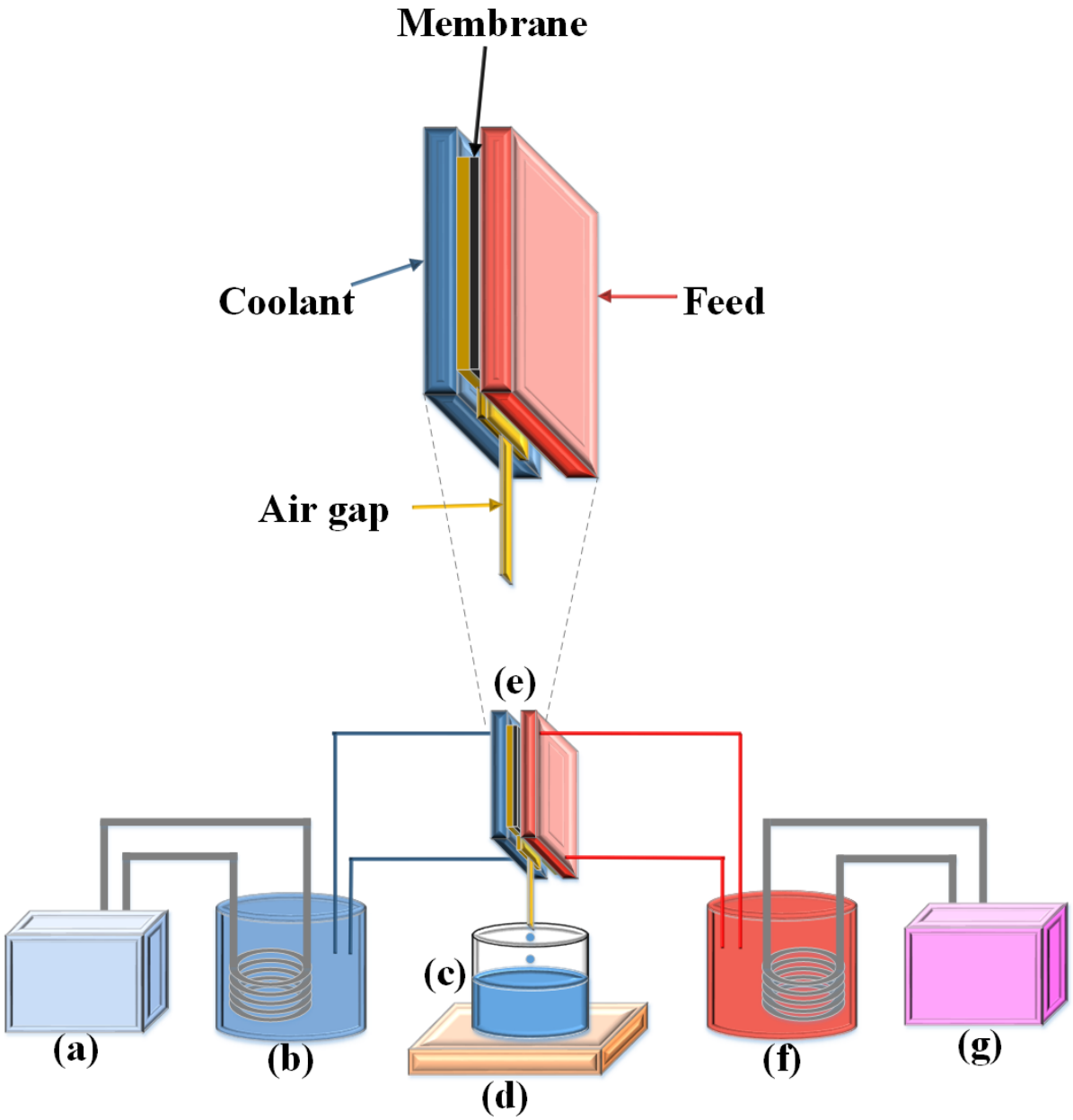

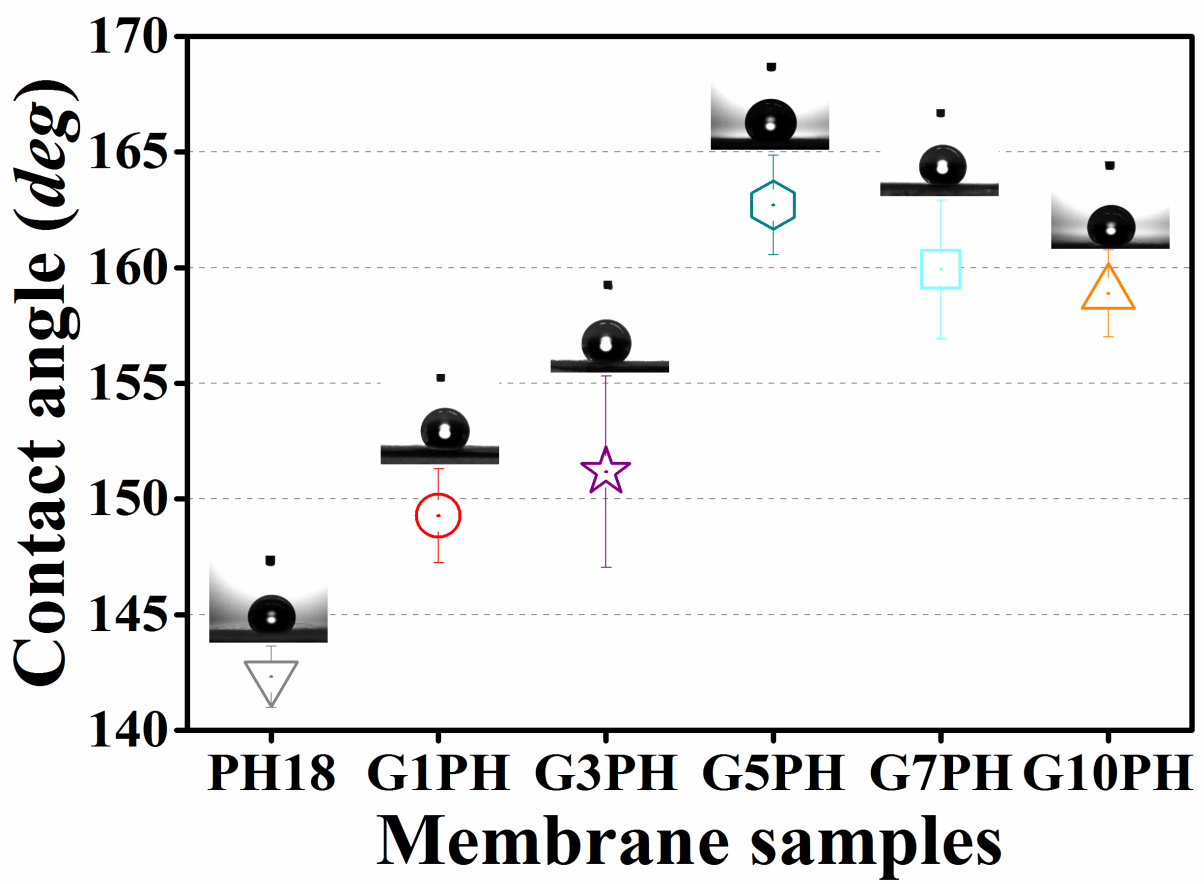

Figure 2 Average contact angle of the fabricated G/PH and neat PH electrospun nanofiber membranes

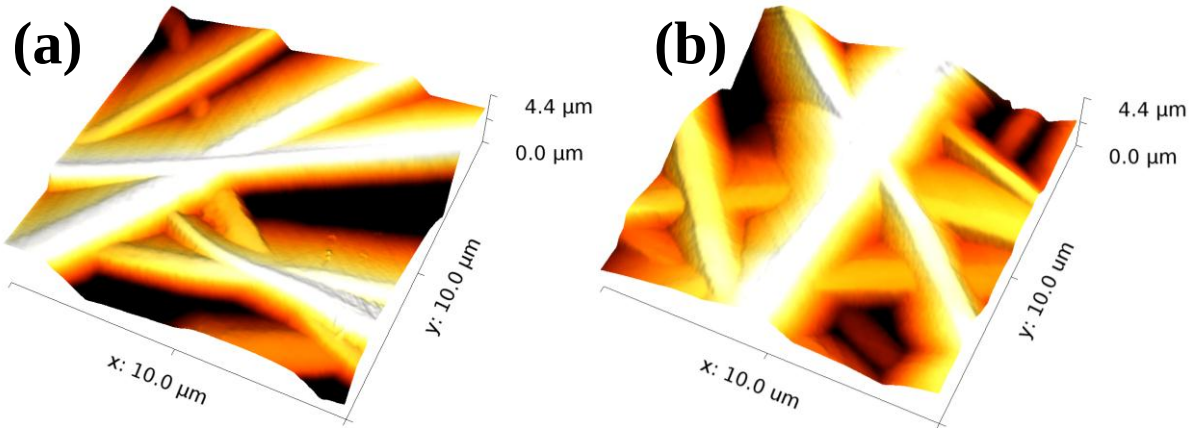

Figure 3 AFM images of (a) the PH18 and (b) the G5PH membranes. The mean roughness (R_a) of the PH18 and G5PH membranes was 0.623 ± 0.01 µm and 0.719 ± 0.03 µm, respectively.

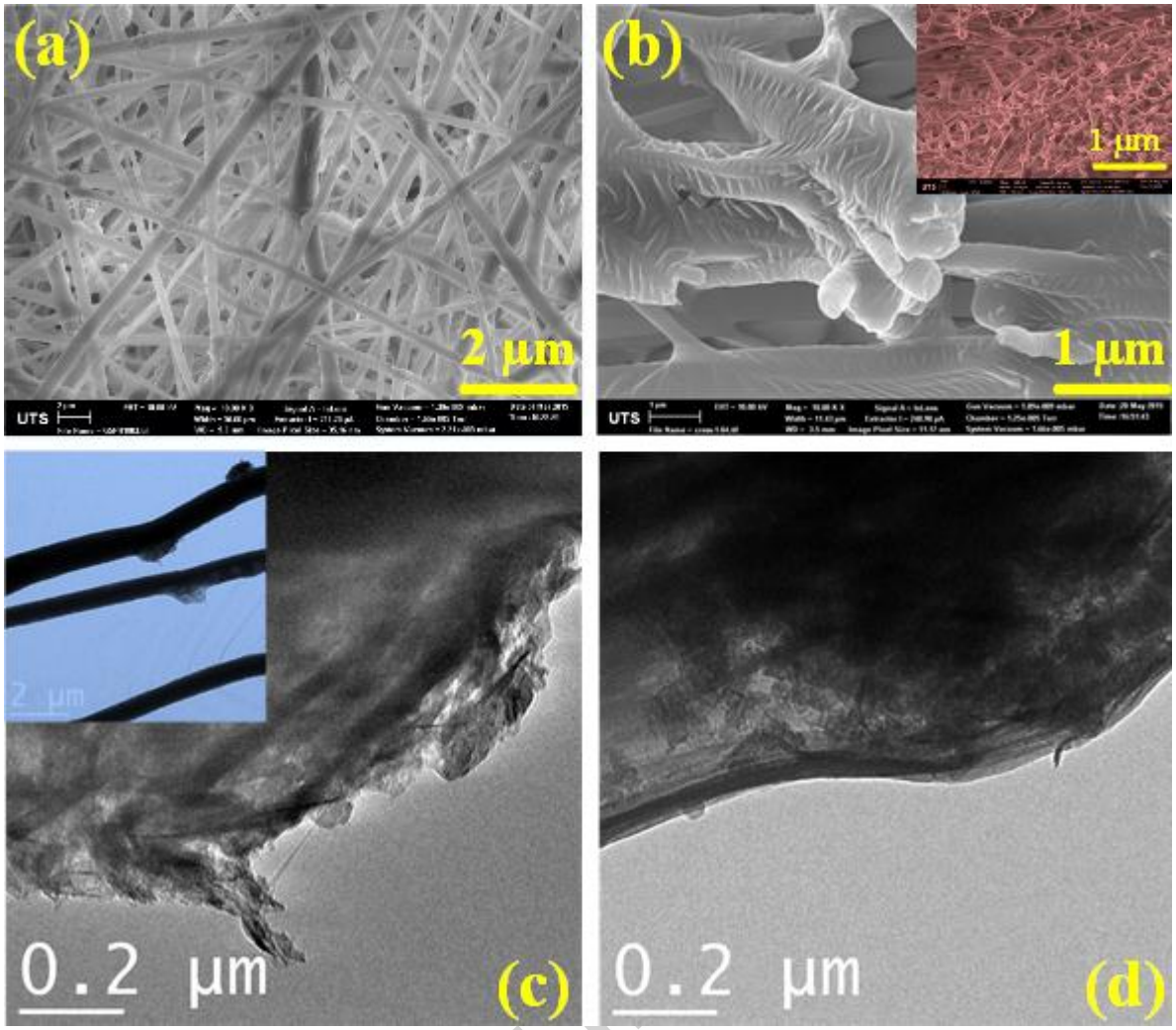

Figure 4 Surface and cross-section morphologies of the G5PH electrospun nanofiber membrane (a and b) by SEM and (c and d) surface morphology of the G5PH electrospun nanofiber membrane by TEM

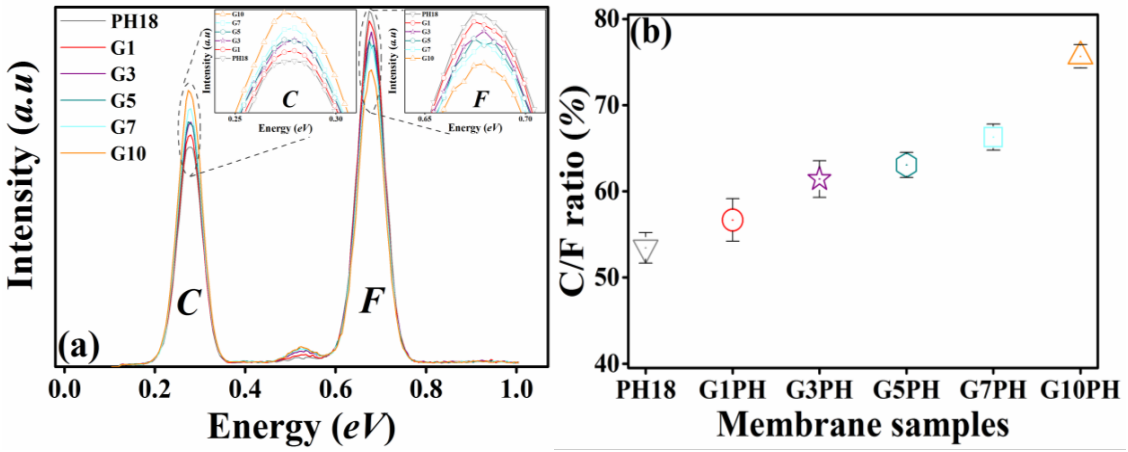

Figure 5 (a) EDX and (b) C/F ratio by EDX of the G/PH and neat PH electrospun nanofiber membranes

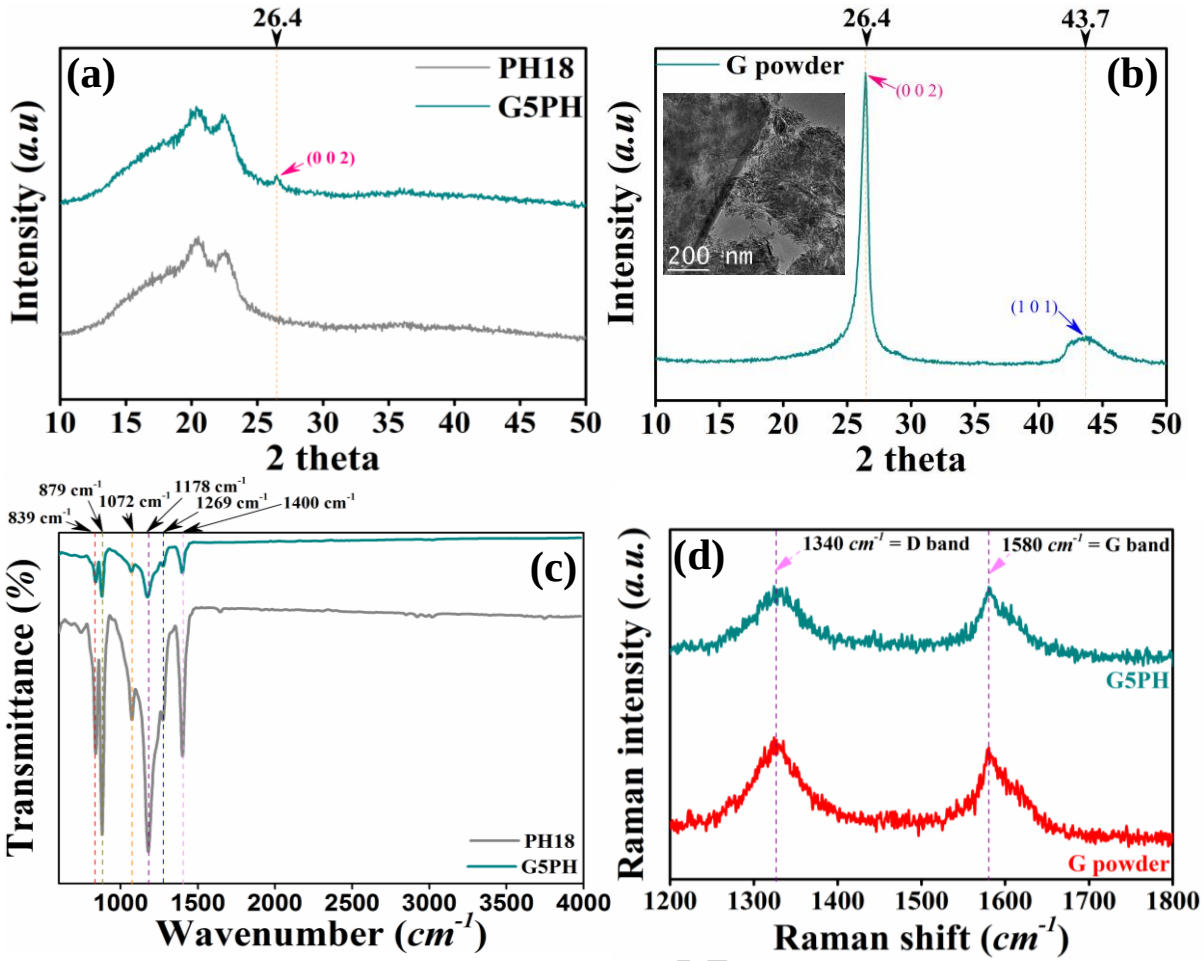

Figure 6 XRD spectra of (a) neat PH and G5PH membranes, and (b) graphene powder; (c) FTIR peaks of neat PH and G5PH membranes, and; (d) Raman spectra of the G5PH membrane and graphene powder

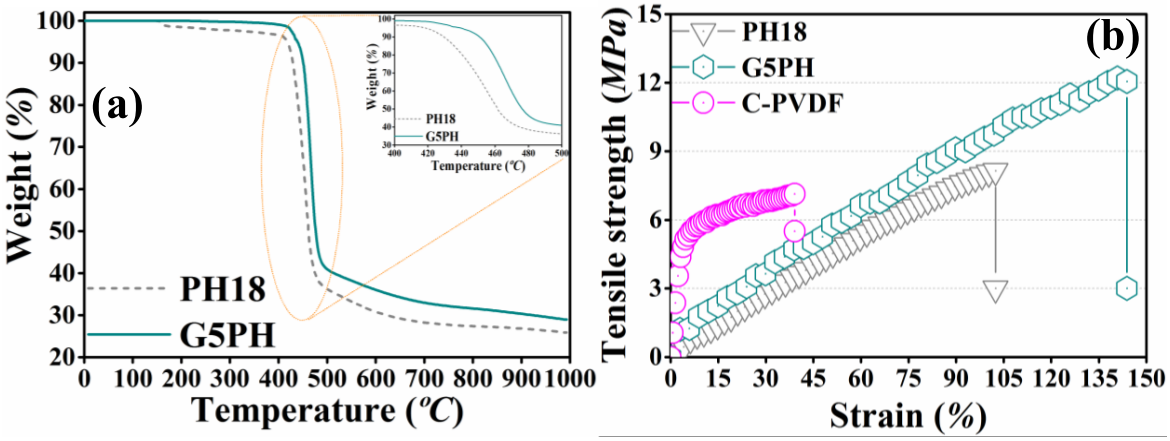

Figure 7 (a) TGA and (b) stress-strain curves of the G5PH and neat PH electrospun nanofiber membranes.

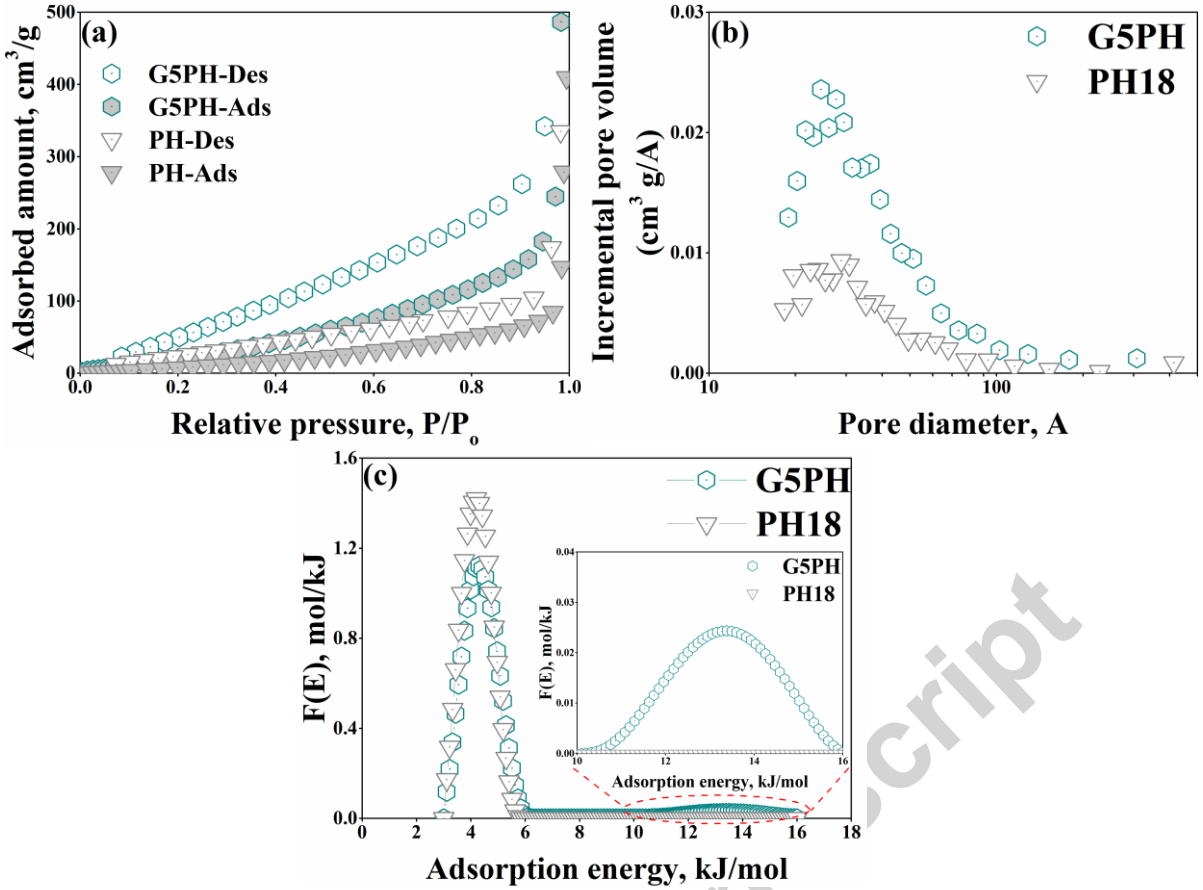

Figure 8 Nitrogen adsorption-desorption isotherms (a) BJH pore size distributions and (b) for G5PH and neat PH membranes and (c) nitrogen adsorption energy distributions on G5PH and neat PH membranes

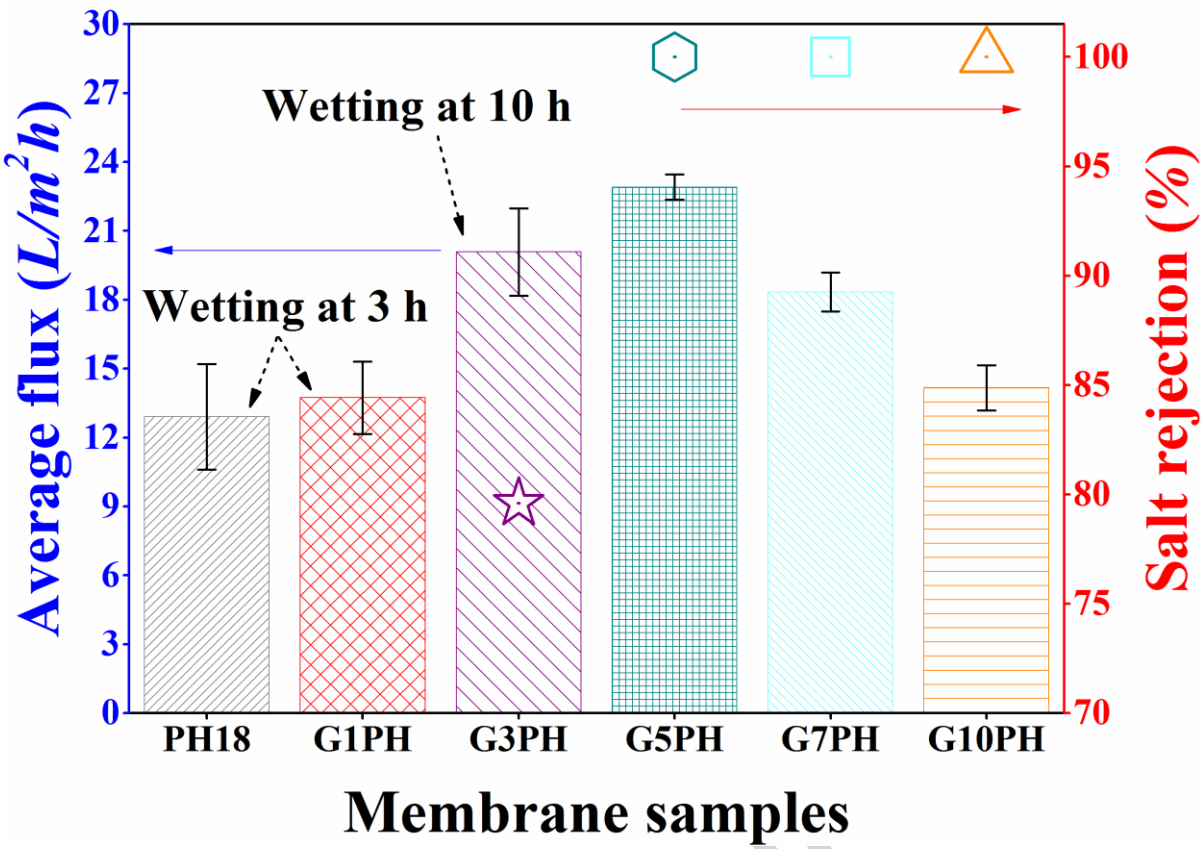

Figure 9 Flux and salt rejection performances of the G/PH and neat PH membranes for 20h operation (Inlet temp at feed = 60°C; Inlet temperature at coolant = 20°C)

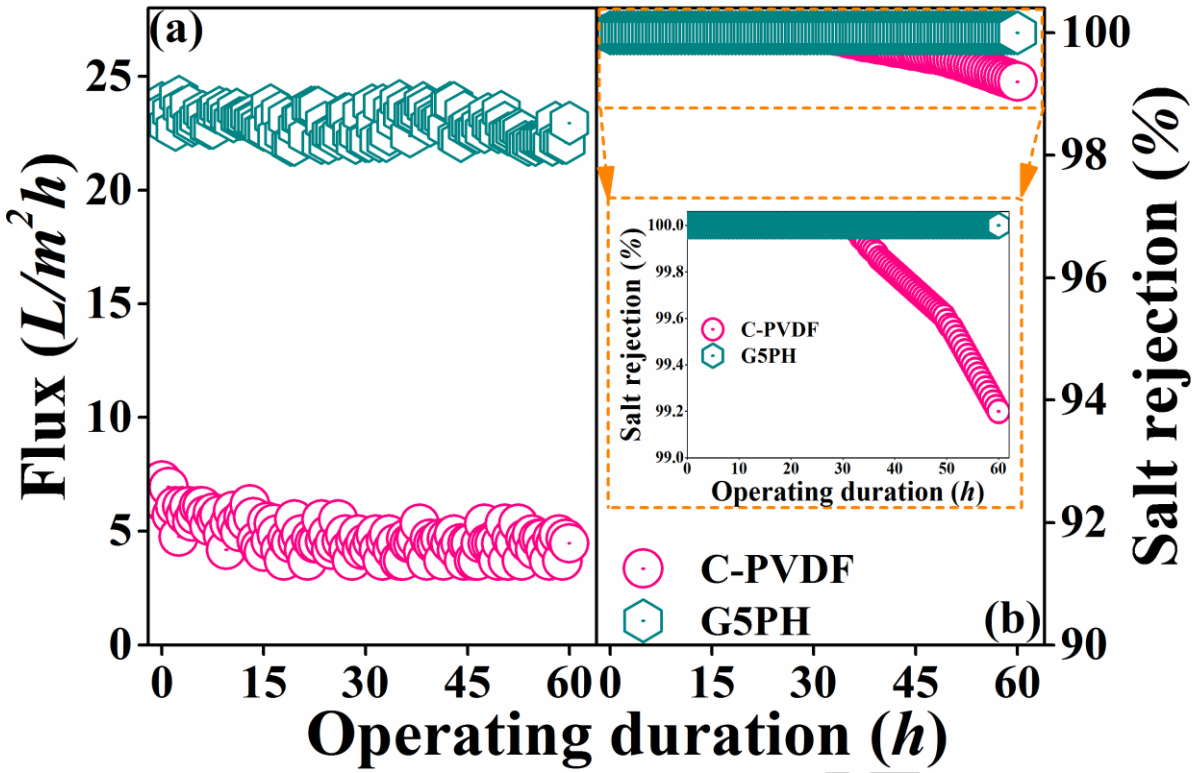

Figure 10 (a) Flux and (b) salt rejection of the G5PH electrospun nanofiber membrane and commercial PVDF membrane

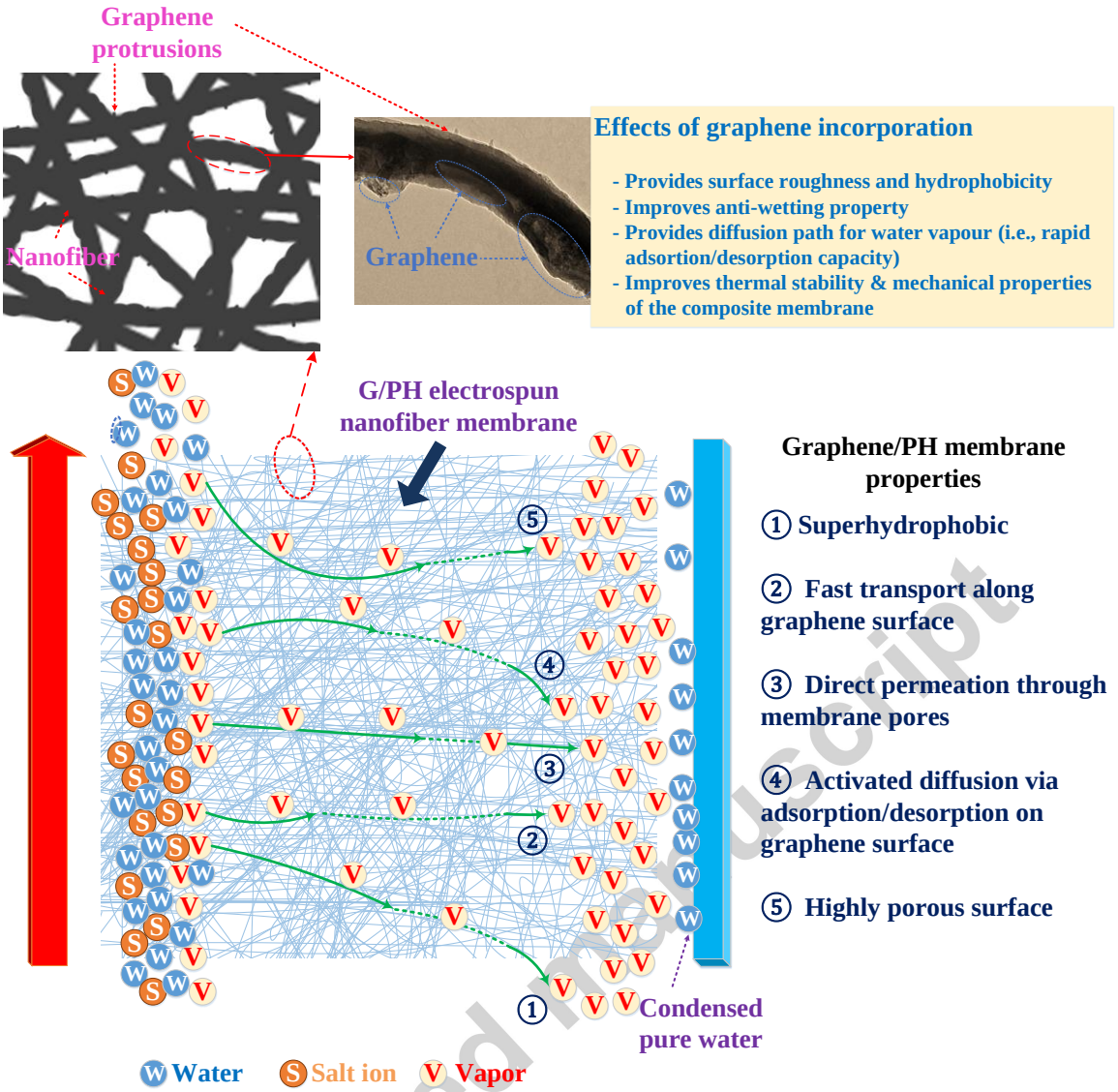

Figure 11 Schematic of the effect of graphene on the membrane for AGMD process

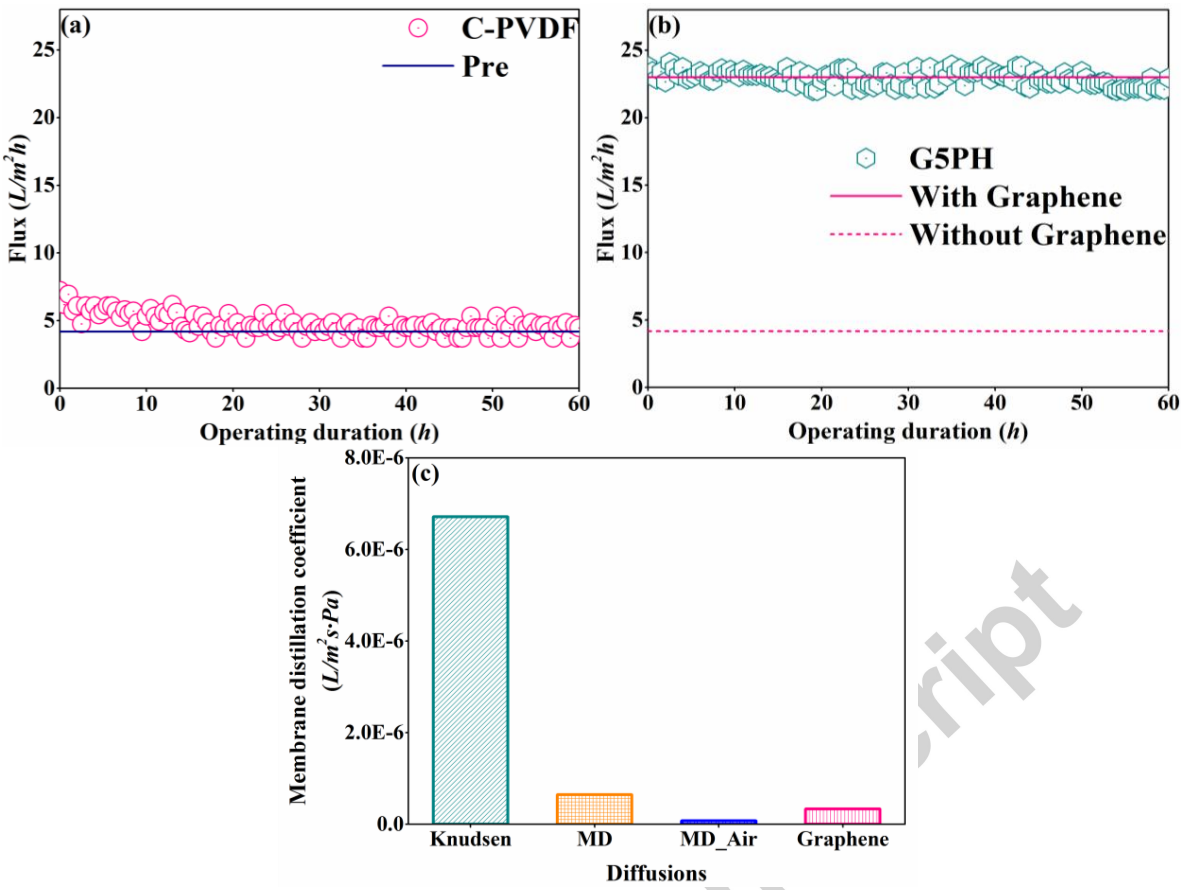

Figure 12 (a) Experimental and predicted flux for commercial PVDF, (b) Predictions for G5PH flux by the AGMD models with and without the presence of graphene sheet and (c) comparison of membrane distillation coefficients for G5PH

Table 1 Characteristics of the neat and G/PH electrospun membranes and commercial membrane

	Membrane thickness (μm)	Mean pore size (μm)	Maximum pore size (μm)	Porosity (%)	LEP (kPa)	Fiber diameter (nm)	Average contact angle (deg)	Tensile strength (MPa)	Elongation at break (%)
PH18	100.1 ± 1.6	0.87 ± 0.03	1.37 ± 0.02	94.7 ± 1.2	139.1 ± 2.5	613.0 ± 130.6	142.3 ± 1.3	2.3 ± 0.2	85.2 ± 0.7
G1PH	100.4 ± 1.9	0.86 ± 0.01	1.38 ± 0.02	92.2 ± 2.8	163.2 ± 2.2	557.1 ± 210.8	149.3 ± 2.0	2.8 ± 0.3	68.2 ± 1.4
G3PH	100.2 ± 0.7	0.83 ± 0.02	1.34 ± 0.03	90.4 ± 1.5	165.8 ± 1.9	359.5 ± 179.5	151.2 ± 4.1	6.3 ± 0.6	146.4 ± 2.2
G5PH	100.2 ± 1.2	0.86 ± 0.02	1.36 ± 0.03	88.7 ± 1.8	186.9 ± 2.4	378.6 ± 144.1	162.7 ± 2.1	12.2 ± 1.2	146.8 ± 2.3
G7PH	100.3 ± 2.4	0.84 ± 0.01	1.35 ± 0.04	84.7 ± 2.4	188.7 ± 3.1	409.1 ± 118.9	159.9 ± 3.0	5.6 ± 0.5	137.8 ± 1.9
G10PH	100.3 ± 1.8	0.85 ± 0.02	1.33 ± 0.03	82.3 ± 2.1	190.3 ± 4.2	429.7 ± 186.4	159.3 ± 1.9	4. 7 ± 0.3	127.1 ± 1.6
C-PVDF [13]	107.4 ± 1.6	0.22 ± 0.02	0.29 ± 0.02	70.3 ± 0.3	213.3 ± 3.1	-	131.1 ± 3.1	7.2 ± 0.2	36.3 ± 3.1

Highlights

- The G/PH membranes are fabricated by a simple electrospinning technique.
- G5PH nanofiber membrane has suitable porosity, pore size, LEP and hydrophobicity for MD.
- G5PH membrane exhibited 4.5 times higher AGMD flux than commercial PVDF membrane.
- G5PH nanofiber membrane showed stable water flux and salt rejection for 60 h.
- Graphene-incorporated nanofiber membranes showed good potential for AGMD desalination.